IMA Journal of Applied Mathematics (2021) **86**, 808–827
https://doi.org/10.1093/imamat/hxab018
Advance Access publication on 30 June 2021

Stationary and oscillatory localized patterns in ratio-dependent predator–prey systems

Fahad Al Saadi
Department of Engineering Mathematics, University of Bristol, Bristol BS8 1UB and Department of Systems Engineering, Military Technological College Oman

Alan Champneys*
Department of Engineering Mathematics, University of Bristol, Bristol BS8 1UB
*Corresponding author: a.r.champneys@bristol.ac.uk

Annette Worthy
School of Mathematics & Applied Statistics, University of Wollongong, Wollongong, Australia

and

Ahmed Msmali
Faculty of Science, Mathematics Department, Jazan University, Jazan, Saudi Arabia

[Received on 15 July 2020; revised on 30 April 2021; accepted on 17 May 2021]

Investigations are undertaken into simple predator–prey models with rational interaction terms in one and two spatial dimensions. Focusing on a case with linear interaction and saturation, an analysis for long domains in 1D is undertaken using ideas from spatial dynamics. In the limit that prey diffuses much more slowly than predator, the Turing bifurcation is found to be subcritical, which gives rise to localized patterns within a Pomeau pinning parameter region. Parameter regions for localized patterns and isolated spots are delineated. For a realistic range of parameters, a temporal Hopf bifurcation of the balanced equilibrium state occurs within the localized-pattern region. Detailed spectral computations and numerical simulations reveal how the Hopf bifurcation is inherited by the localized structures at nearby parameter values, giving rise to both temporally periodic and chaotic localized patterns. Simulation results in 2D confirm the onset of complex spatio-temporal patterns within the corresponding parameter regions. The generality of the results is confirmed by showing qualitatively the same bifurcation structure within a similar model with quadratic interaction and saturation. The implications for ecology are briefly discussed.

Keywords: predator–prey; localized patterns; Hopf bifurcation; Turing instability; spatio-temporal chaos.

1. Introduction

Spatial ecology is a relatively recently introduced term for the study of spatial effects in ecology, see Fletcher & Fortin (2018) for an overview. As originally introduced by Tilman & Kareiva (1997), the term mostly refers to statistical methodologies for studying the autocorrelation of ecosystems in different spatial locations, as well as the effect of landscape change and animal movement. However, the study of spatial effects in ecological models actually goes back much further than that, see e.g. the groundbreaking work of Skellam (1951) who set the scene for hypotheses on dispersal that have been studied extensively in the past few decades. Before that, there was the pioneering work independently by Fisher, Kolmogorov, Pitrovski and Piskunov in 1937 that led to the famous K-KPP reaction–diffusion model that is known to support travelling wave fronts, see e.g. Grindrod (1996) and references therein.

There is now a rich literature within theoretical ecology of models that can give rise to complex spatio-temporal patterns.

The particular question of interest in this paper is whether predator–prey interaction can give rise to stable spatial hotspots, which is temporally stable localized patterns of high or low population density within a homogeneous environment. There are comparatively fewer studies that consider theories for such patterns in ecological systems. Notable exceptions are early works by Okubu & Levin (2001); see also Meron (2015) and references therein. There is also recent theoretical work seeking to explain vegetation patterns in semi-arid zones (e.g. Bastiaansen *et al.*, 2018; Gandhi *et al.*, 2018; Meron, 2019; or rainforest-savanna systems; Wuyts *et al.*, 2017).

The context in which we choose to address this question is that of classical predator–prey systems, where typically the interaction times are faster than many of the vegetation-pattern models. In the late 1950s and early 1960s, Holling (1959, 1965) postulated three different types of functional relationships between predator and prey, from a simple multilinear interaction (type I), to rational Hill-type nonlinearities of power 1 (type II) or higher (type III). See Dawes & Souza (2013) for a modern rigorous definition of these kinds of nonlinear terms as the limits of random processes. Actually, type II functional responses were first considered by Rosenzweig & MacArthur (1963). The existence of Hopf bifurcations in this model is ecologically significant, especially because the bifurcation occurs as the prey carrying capacity is increased. This is known as the paradox of enrichment Rosenzweig (1971) and Roy & Chattopadhyay (2007) for which spatial dispersal has been argued as one solution, at least on some timescales (Grindrod, 1988). In fact, it has been known for almost 30 years that this model, when spatially extended by diffusion, can exhibit spatio-temporal chaos (Pascual, 1993).

We also restrict attention to models that use simple second-order diffusion to model random dispersal of spatially structured populations, which is at best only an approximation to how real populations move. See e.g. the review by Potts & Lewis (2019) for models that incorporate territoriality, home-range analysis and other kinds of taxis in pattern-forming behaviours where demographics (birth and death) can be ignored. Others have considered slightly longer timescales and thus included demography alongside more complicated models of movement than random dispersal, see e.g. Taylor *et al.* (2020) and references therein. Typical models of vegetation pattern formation in semi-arid landscapes also involve more complicated spatial effects such as advection of water. In what follows, we shall take a parsimonious approach and ignore such complexities, while considering an intermediate timescale where demography is important, but not so long as in the case of vegetation pattern formation.

Another motivation for the present work is the recent interest in the propensity for localized structures in a multitude of different settings that are governed by systems of reaction–diffusion equations; see e.g. Knobloch (2015) and Champneys *et al.* (2021) for reviews. Such structures appear from the subcritical Turing bifurcations that emerge due to the bi-stability between homogeneous rest states and spatially periodic patterned state. The existence of such localized patterns has been observed in various area of study whenever there is an active medium and include chemical reactions, many areas of fluid mechanics and soft matter, optical systems and even a theory of crime hot spots (Lloyd & O'Farrell, 2013; Tes & Ward, 2016).

Of particular relevance here are several recent theories for spontaneous creation of localized vegetation patterns (Bastiaansen *et al.*, 2019; Dawes & Williams, 2016; Meron, 2016, 2018; Zelnik *et al.*, 2013). Indeed such localized patches have been reported in various study areas such as marine sea-grasses (Ruiz-Reynés *et al.*, 2017) and drylands (Lejeune *et al.*, 2002; Zelnik *et al.*, 2013, 2016).

Here though we shall focus on localized patterns in predator–prey systems, where in addition to spatially periodicity, through a Turing bifurcation, one can have temporal periodicity through a Hopf bifurcation. Our study was originally inspired by the works of Borgogno *et al.* (2009), Bordeu *et al.*

(2016) and Cobbold *et al.* (2015), which study predator–prey-like models that might underlie the onset of spatio-temporal patchiness. Our analysis is also in the same spirit as recent relevant bifurcation analyses such as in the works of Mukherjee *et al.* (2018), Xiao & Jennings (2005), Bandyopadhyay & Chattopadhyay (2005), Jiang *et al.* (2017) and Medvinsky *et al.* (2002). In particular, in the context of Holling type-II and III predator–prey models, we mention the works of Berezovskaya *et al.* (2001) and Hsu *et al.* (2001). Also the existence of Turing patterns and the chaos was considered in Banerjee & Petrovskii (2011) and Medvinsky *et al.* (2002) and the existence of stable limit cycle was shown in Xiao & Ruan (2001).

The rest of this paper is organized as follows. Section 2 presents a system of reaction-diffusion equations that represent a predator–prey model with a modified Holling type-II nonlinearity. That section also contains linear and weakly nonlinear analysis to identify the co-dimension two point where pattern onset through a Turing bifurcation changes from subcritical to supercritical. Section 3 then contains numerical bifurcation analysis for the system posed on a long 1D domain, where so-called homoclinic snaking causes multistable patterns with arbitrarily many patches. The effect of a temporal supercritical Hopf bifurcation is shown to lead to spatio-temporal chaos. Furthermore, Section 4 studies the same model numerically in two spatial dimensions, and evidence is found of 2D localized patterns and spatio-temporal chaos for similar parameter values. Section 5 shows that qualitatively similar results can be found in a generalized Holling type-III ratio-dependent model. Finally, Section 6 contains concluding remarks.

2. A ratio-dependent predator–prey model

Consider the ratio-dependent predator–prey reaction–diffusion system of nonlinear partial differential equations (PDEs) studied in Kuang & Beretta (1998):

$$u_t = f(u,v) + \epsilon\nabla^2 u = u(1-u) - \frac{\beta uv}{u+v} + \epsilon\nabla^2 u, \tag{2.1a}$$

$$v_t = g(u,v) + \nabla^2 v = \frac{\alpha uv}{u+v} - \delta v + \nabla^2 v. \tag{2.1b}$$

Here $u(z,t)$ and $v(z,t)$ represent, respectively, dimensionless prey and predator population densities at position z. In what follows, we shall consider the problem in one spatial dimension, in which case $z = x$ or in 2D, in which case (x,y). We assume that the domain is large and there are homogeneous Neumann boundary conditions at $x = \pm L$ and, if appropriate, $y = \pm L$ for some $L \gg 1$.

The parameters in (2.1) can be interpreted as follows: α is a conversion coefficient that measures the positive effect of the predator's interaction with the prey, β is the corresponding negative effect on the prey, δ is ratio of net death rate of the predator to the birth rate of the prey in the absence of interaction and $\epsilon \ll 1$ is the ratio of diffusion of the relatively static prey to the much more mobile predators. When applied to vegetation patches, u and v represent vegetation and the environment, respectively.

In the absence of the diffusion terms in (2.1), a straightforward calculation shows that the solution (u,v) admits three homogeneous steady-state points. These being

(i) The extinct steady-state $S_1 = (0,0)$.

(ii) The predator-free steady-state $S_2 = (1,0)$.

(iii) The coexistence steady-state $S_3 = (u^*, v^*)$ with

$$u^* = \frac{\beta\,(\delta-\alpha)+\alpha}{\alpha}, \quad v^* = \frac{u^*\,(\delta-\alpha)}{\delta} \tag{2.2}$$

exists under the following conditions $\alpha > \beta(\alpha-\delta)$ and $\delta > \alpha$.

Several authors, e.g. Xiao & Ruan (2001) and Banerjee & Volpert (2017), have considered how ratio-dependent predator–prey systems require some additional rule in order to be well defined at the origin. In our case, the trivial steady-state S_1 is at the edge of the allowed domain for (u, v) and is unstable in all parameter regions we investigate. From a biological perspective, we are interested in localized patterns that have as background the non-zero steady-state S_3.

To develop a basic analytical understanding, we first consider (2.1) in one spatial dimension only. Hence, for the remainder of this section, we will shall assume $\nabla^2 = \frac{\partial^2}{\partial x^2}$.

2.1 *Linear stability analysis*

The Jacobian matrix of the system linearized about the equilibrium S_3 is

$$J = \begin{pmatrix} \frac{(\beta-1)\alpha^2-\beta\,\delta^2}{\alpha^2} & -\frac{\beta\,\delta^2}{\alpha^2} \\ \frac{(\alpha-\delta)^2}{\alpha} & -\frac{(\alpha-\delta)\delta}{\alpha} \end{pmatrix}. \tag{2.3}$$

A straightforward analysis of the eigenvalues of J reveals that a Hopf bifurcation occurs at the critical value of $\alpha = \alpha_H$ given by

$$(\beta-\delta-1)\,{\alpha_H}^2 + \delta^2\left(\alpha_H - \beta\right) = 0. \tag{2.4}$$

Next, to look for a pattern-formation, or Turing, instability of S_3, we follow a standard approach (e.g. Cross & Hohenberg, 1993) by considering the ansatz

$$\begin{pmatrix} u \\ v \end{pmatrix} = \begin{pmatrix} u^* \\ v^* \end{pmatrix} + \begin{pmatrix} a_k \\ b_k \end{pmatrix} e^{ikx+\lambda t}, \tag{2.5}$$

where k and λ are the spatial wave number and the growth factor or temporal eigenvalue, respectively, and a_k and b_k are the real amplitudes with solution $\|(a_k, b_k)\| \ll 1$. The corresponding dispersion relation is

$$\lambda(k)^2 - T_k\lambda(k) + D_k = 0 \tag{2.6}$$

where

$$T_k = \frac{\left(\beta-(\delta+1)-(\epsilon+1)\,k^2\right)\alpha^2+(\alpha-\beta)\;\delta^2}{\alpha^2}$$

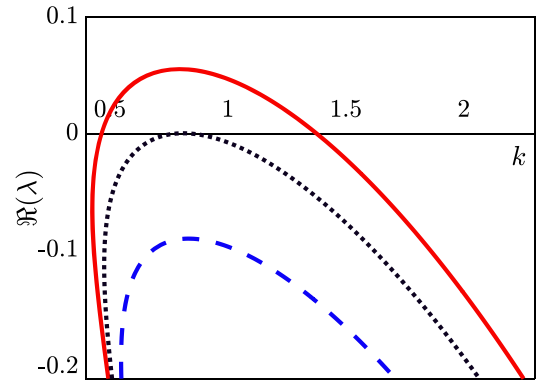

FIG. 1. Dispersion curves $\Re(\lambda)$ in (2.6) versus k for $\beta = 2.3$, $\delta = 0.3$, $\epsilon = 0.1$ and three different bifurcation values of α: $\alpha = 0.4$ (solid red line), $\alpha = 0.39188$ (dotted black line) and $\alpha = 0.390$ (dashed blue line).

and

$$D_k = \frac{\left(k^2+\delta\right)\left(\epsilon k^2-\beta+1\right)\alpha^2-\delta^2\left(\epsilon k^2-2\,\beta+1\right)\alpha+\beta\,\delta^2\left(k^2-\delta\right)}{\alpha^2}.$$

From (2.6), we have $\lambda(k) = \frac{T_k \pm \sqrt{T_k^2-4D_k}}{2}$. The solution is stable whenever $\Re(\lambda) < 0$ for all k and the conditions for a Turing instability with critical wave number k_c is

$$\Re(\lambda(k_c)) = 0 \quad \text{and} \quad \Re(\partial_k \lambda(k)|_{k=k_c}) = 0. \tag{2.8}$$

Note that S_3 is stable for the spatially homogeneous mode $k = 0$.

Applying (2.8) to (2.6), we find

$$(-\epsilon\delta+\beta-1)\,\alpha^2+\delta^2\,(\alpha\,\epsilon-\beta) = 2\,\alpha\,\sqrt{\epsilon\,\delta\,\,(\alpha-\delta)\,(\beta\,\,(\delta-\alpha)+\alpha)}, \tag{2.9a}$$

$$k_c^2 = \frac{(-\epsilon\delta+\beta-1)\,\alpha^2+\delta^2\,(\alpha\,\epsilon-\beta)}{2\alpha^2\epsilon}. \tag{2.9b}$$

Thus, (2.9) gives the value $k = k_c$ and the parameter condition for Turing instability. Figure 1 displays various dispersion curves for $\Re(\lambda)$ in (2.6) versus k for specific values of the parameters β, δ and ϵ while varying the bifurcation parameter α. The figure shows different scenarios of solution stability for (2.1). Specifically, $\alpha > \alpha_c$ (solid red curve) represents instability where there are positive eigenvalues λ for a range of k-values, $\alpha = \alpha_c$ (dotted black curve) represents the critical case of a Turing bifurcation where for $k = k_c$ $\lambda = 0$ and $\frac{d\lambda}{dk} = 0$ and $\alpha < \alpha_c$ (blue dashed curve) which corresponds to instability as $\lambda < 0$ for all k.

Moreover, we obtain the following condition for the existence of double real spatial eigenvalue (sometimes referred to as a Belyakov–Devaney (BD) transition,

$$(-\epsilon\delta+\beta-1)\,\alpha^2+\delta^2\,(\alpha\,\epsilon-\beta) = -2\,\alpha\,\sqrt{\epsilon\,\delta\,\,(\alpha-\delta)\,(\beta\,\,(\delta-\alpha)+\alpha)} \tag{2.10}$$

the significance of which is explained in the next section.

2.2 *Weakly nonlinear analysis*

We now seek an analytical expression for the codimension-two point for (2.1) where the Turing bifurcation changes from a super to subcritical bifurcation. This is achieved by using normal form analysis (Elphick *et al.*, 1987; Haragus & Iooss, 2007; Verschueren & Champneys, 2017). Consequently, we introduce a new set of variables (U, V) into (2.1) centered on the steady-state S_3:

$$\begin{pmatrix} u \\ v \end{pmatrix} = \begin{pmatrix} u^* \\ v^* \end{pmatrix} + \begin{pmatrix} U \\ V \end{pmatrix} \tag{2.11}$$

where u^*, v^* represents the steady-state S_3. Hence, we obtain

$$\begin{pmatrix} U \\ V \end{pmatrix}_t = \left[J|_{S_3} + D\partial_{xx} \right]_c \begin{pmatrix} U \\ V \end{pmatrix} + \begin{pmatrix} U \\ V \end{pmatrix} NL(U, V), \tag{2.12}$$

where $\left[J|_{S_3} + D\partial_{xx} \right]_c$ represents the linear operator of (2.12) with J being the Jacobian matrix evaluated at S_3, D is a diagonal matrix that accounts for the diffusion coefficients associated with the second-order spatial derivatives and $NL(U, V)$ is a scalar quantity that reflects the nonlinear terms in (2.1) after using the change of variables (2.11). Here, the sub-index c is referring to the critical values of the parameters (α, ϵ), which are determined by (2.9) for fixed β and δ. In the rest of the analysis, we will drop the sub-index c assuming that all functions are evaluated at the critical values of these parameters.

We follow Elphick *et al.* (1987) to determine the coefficients of the normal form and use a similar procedure of that in Verschueren & Champneys (2017) for our given system of equations (2.12). The details are omitted for brevity. We seek a time-independent solution for (2.12) of the form

$$\left. \begin{pmatrix} U \\ V \end{pmatrix} \right|_{lin} = \left(A e^{ik_c x} + c.c. \right) \begin{pmatrix} w_1 \\ w_2 \end{pmatrix}, \tag{2.13}$$

where $k = k_c$ is at the critical value of parameters (α, ϵ), $c.c.$ means the complex conjugate, w_i, $i = 1, 2$ are obtained from the Ker $\left(J + D\partial_{xx} \right)$ in (2.12) and A is the constant amplitude of the pattern. At third order, we obtain an amplitude equation of the form

$$\partial_t A = L_1 A + L_3 A|A|^2 + O(A|A|^4), \tag{2.14}$$

where the L_i are normal form coefficients that can be expressed in terms of all the parameters of the problem. These expressions are lengthy but can easily be evaluated using computer algebra. Using the algebraic expressions so obtained, Fig. 2a plots the value of L_3 as a function of the single variable α with $\epsilon = \epsilon(\alpha)$. The point $L_3 = 0$ is indicated by a yellow circle. This represents a codimension-two point where the Turing bifurcation changes from being subcritical (red) to a supercritical (blue). Figure 2b presents the location of the codimension-two point in the (ϵ, α)-plane. The importance of the existence of a subcritical region is that this leads to a bi-stability region between the homogeneous state and the bifurcating periodic patterned state in which we might expect to find localized structures.

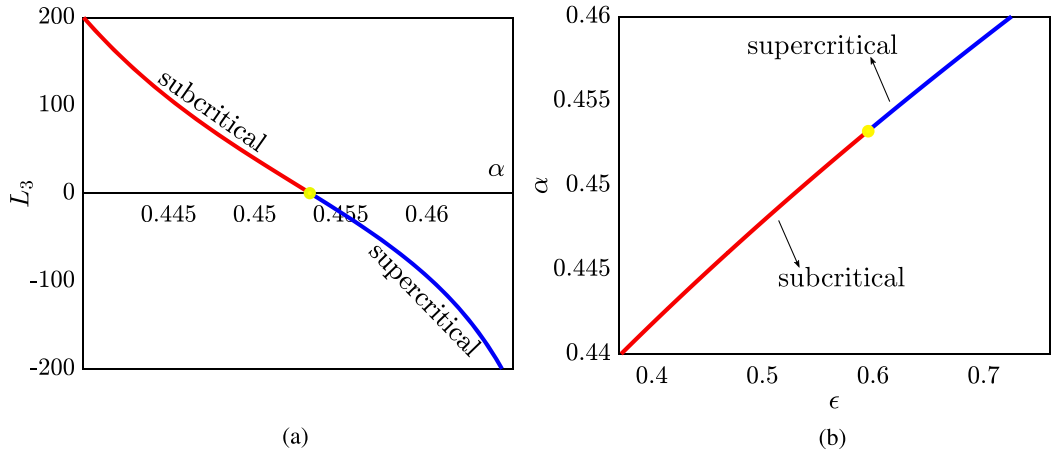

FIG. 2. The fixed parameters values of $\beta = 2.3$ and $\delta = 0.3$ are used. (a) A plot of $L_3 = L_3(\alpha)$ where the yellow coloured circle indicates the zero of L_3. (b) A plot of ϵ versus α along the critical curve in (2.9) where the codimensional-two point $(\epsilon_c, \alpha_c) = (0.6044768459, 0.4537)$ is indicated by the yellow coloured circle. In both figures, the coloured yellow circle indicates that there is a change in Turing bifurcation from being subcritical (red curve) to supercritical (blue curve).

3. Bifurcation analysis and numerical simulation

We now use the local bifurcations in the previous section as the starting point of an investigation into localized pattern solutions to (2.1). These are solutions that asymptote to the coexistence homogeneous state. In what follows, unless otherwise stated, we fix

$$\beta = 2.3, \qquad \delta = 0.3 \tag{3.1}$$

and treat α and ϵ as bifurcation parameters.

3.1 *Numerical methods*

The suite of numerical tools used to investigate localized pattern solutions to (2.1) is the same as used in earlier papers by the first two authors, e.g. Champneys *et al.* (2021) and Al Saadi *et al.* (2021a,b).

Accurate computation of steady solutions as parameter vary is undertaken using the numerical continuation package AUTO. To do this, we truncate to a long finite domain $[-L, L]$ where $L \gg 1$. Standard theorems on numerical approximation of homoclinic solutions (Sandstede, 1997) show that in the case that the far field represents a hyperbolic equilibrium, then the convergence is exponential in L. Also, without loss of generality, we solve on the half domain $[0, L]$ for $L \gg 1$ with Neumann boundary conditions. This is because the steady version of (2.1) on the real line can be written as a reversible system, but it does not conserve a first integral. Therefore, symmetric homoclinic orbits (satisfying Neumann boundary conditions at their mid point) are generic under parameter perturbation, whereas asymmetric homoclinic orbits are not structurally stable (see e.g. Champneys, 1998, and references therein). Typically, we use values of $L = 200$ but we often choose to depict only the portion of the solution close to $x = 0$. Sometimes, for convenience, we also depict solutions for $x < 0$ also, which is obtained by symmetry.

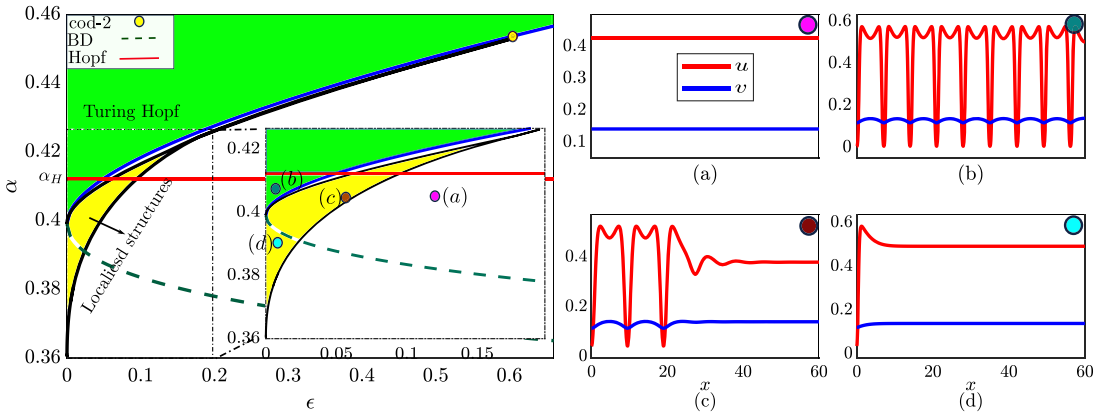

FIG. 3. (Left): bifurcation diagram of (ϵ, α) with white, green and yellow coloured regions to identify the different types of solution $(u(x), v(x))$ for (2.1). All solution curves are obtained analytically except thin black lines which are a numerically contained curve of folds of the single-patch localized structure shown in panel (d). In addition above the Hopf bifurcation line (red curve) steady-state solutions are unstable to an oscillatory instability. (Right): solution profiles of typical steady state at the points labelled (a)–(d) in the left-hand plot.

To look at the stability and dynamics of localized patterns, we use a dual approach in Matlab. We compute stability by taking a second-order finite-difference approximation to the PDE system linearized about one of the non-trivial steady states, extended to a symmetric domain $[-L, L]$. We then compute the spectrum of the resulting discretized inhomogenous linear operator using Matlab routine `eig`. Care was taken to allow both symmetric and anti-symmetric eigenmodes.

In addition, we simulate of the fully nonlinear PDE system obtained using the same finite-difference approximation in space, with zero flux boundary conditions, using the Matlab stiff solver `ode15s`. Typical values of the maximum temporal and spatial step sizes were chose as $\mathrm{d}t = 0.001$ and $\mathrm{d}x = 0.05$, respectively, so as to satisfy the CFL stability conditions. Care was taken to check that the results presented are qualitatively robust to changes in L and in the step sizes and Matlab tolerance parameters.

3.2 *Parameter space investigation in 1D*

Figure 3 depicts an overall summary of the two-parameter bifurcation diagram, indicating the linear stability boundaries and parameter regions where different kinds of solution are observed. The particular curves plot consists of several boundaries: the Hopf bifurcation of S_3 (red line) given by (2.4), the Turing bifurcation (blue) (2.9), the BD transition curve (dashed green) (2.10) and the boundary of the parameter regime in which we numerically find localized structures (black lines). It is clear that the Hopf line divides the bifurcation diagram into two parts: $\alpha > \alpha_H$ where solutions are unstable to a global (spatially uniform) oscillatory mode and $\alpha < \alpha_H$ where solutions are stable to such perturbations.

Also in the figure are three coloured regions that identify various types of steady-state solution for (2.1). These regions are classified as follows: stable homogeneous solution region (white), periodic spatial pattern region (green) and the 'pinning region' (yellow) in which localized structures occur. Note that the localized structure region is separated into three pieces by the BD transition curve and the Hopf bifurcation line, whereas the periodic-pattern region is divided into two parts by the Hopf line. Note the yellow circle which represents the codimension-two point (ϵ_c, α_c) found in Section 2.2 where the Turing bifurcation changes critically. We see that this is the origin of the (yellow) localized structure region,

which becomes exponentially thin as it approaches this point, just as predicted by the theory (Kozyreff & Chapman, 2006).

The right-hand plots in Fig. 3 illustrates four different types of steady-state solution at parameter values represented in the left-hand diagram. All points are taken for $\alpha < \alpha_H$ where the solutions are stable to the global Hopf mode.

Point (a), $(\epsilon, \alpha) =$ for $(0.11, 0.413)$, represents the unique attracting solution in the white parameter region which is the coexistence homogeneous equilibrium S_3.

Point (b) has $(\epsilon, \alpha) = (0.01, 0.409)$ represents a typical solution from the green parameter region of large-amplitude spatially (quasi-) periodic patterns. The nature of the pattern here is that of a multi-scale pattern in which there are repeated patches in which the population $u(x)$ of prey is significantly reduced. Note that the precise pattern observed on a long domain is a delicate function of parameters and domain size, as is well known in the theory of Turing patterns (see e.g. Maini *et al.*, 1997; Murray, 2002). A difference here from the usual case, owing to the subcritical Turing bifurcation, is that there is no stable small-amplitude pattern close to the Turing bifurcation. Instead, fully formed large-amplitude patterns emerge from a fold bifurcation (close to the outer black line delineating the yellow pinning region).

Point (c), for $(\epsilon, \alpha) = (0.05, 0.408)$, is an example of a localized structure from within the yellow parameter region above the BD line. Such solutions with an arbitrary finite number of large-amplitude u-oscillations within a background of the homogeneous state S_3 coexist with fully periodic solutions. Note that above the BD curve corresponds to where localized solutions have oscillatory tails. Typically, such solutions lie on snaking bifurcation diagrams, as explained in the next subsection.

Finally, point (d), for $(\epsilon, \alpha) = (0.013, 0.39)$, shows an example of a single isolated peak solution within the yellow region beneath the BD curve. Here there is a single isolated patch of prey degradation which has monotonic decay to the homogeneous steady-state S_3. The mechanism of transition between such localized structures and single-peak states across the BD curve seems to occur via exactly the same process that was explained in Verschueren & Champneys (2021).

3.3 *Homoclinic snaking and instability of localized patterns*

Figure 4 shows a one-parameter bifurcation diagram with α of localized structures from the yellow parameter region of Fig. 3 above the BD curve. The norm used is vector $L_2 -$ norm of u, v and their first spatial derivatives. Representative solution profiles and their spectra are depicted in Fig. 5. Several features can be observed from these two figures, which we now explain.

The first feature to note is the usual snaking structure that is typically observed within a Pomeau pinning region that emerges from a subcritical Turing bifurcation (Beck *et al.*, 2009; Knobloch, 2015; Kozyreff & Chapman, 2006; Woods & Champneys, 1999). The inner and outer extent of the pinning region is delineated by the accumulation of the fold curves on the left- and right-hand sides of the snaking diagram. Following one of these folds in two parameters results in the black lines that delineate the yellow region in Fig. 3. Note the intertwined nature of the curves on which patterns exist with even and odd numbers of patches. There are stationary no 'rung states' (curves of asymmetric stationary localized patterns) in this case because, although the system in question is spatially reversible, it does not have variational structure (see Knobloch, 2015, and references therein for this distinction). At every successive fold bifurcation, each of the branches loses stability or regains it in a fold bifurcation.

The additional feature of this snaking bifurcation diagram, which is not present in other studies, is the presence of the Hopf bifurcation of the background state that cuts the bifurcation diagram in two. A natural question would be to seek to understand the relation between the Hopf bifurcation of the background state and a corresponding instability of the localized states. From the figures, it is clear that

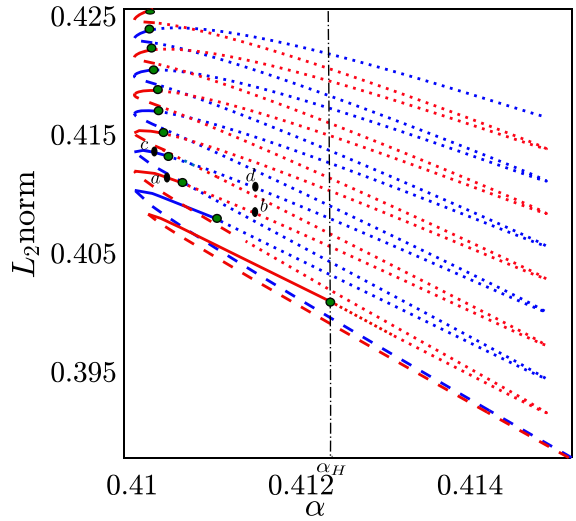

FIG. 4. Numerical bifurcation diagram showing paths of localized structures for $\epsilon = 0.085$ as α varies. Red/blue lines indicate solutions with an odd/even number of localized patches. Profiles and spectra of solutions at the points labelled a to d are depicted in Fig. 5. The vertical dashed line $\alpha = \alpha_H$ indicates the Hopf bifurcation of the homogeneous solution S_3. Green dots indicate Hopf bifurcation points causing loss of stability of localized structures. More generally, stability information is encoded in the line type: continuous lines represent stable branches, whereas the dashed lines represent branches that are unstable to a real-eigenvalue instability (through a fold in the homoclinic snake) and dotted lines indicate branches that are unstable to an oscillatory instability.

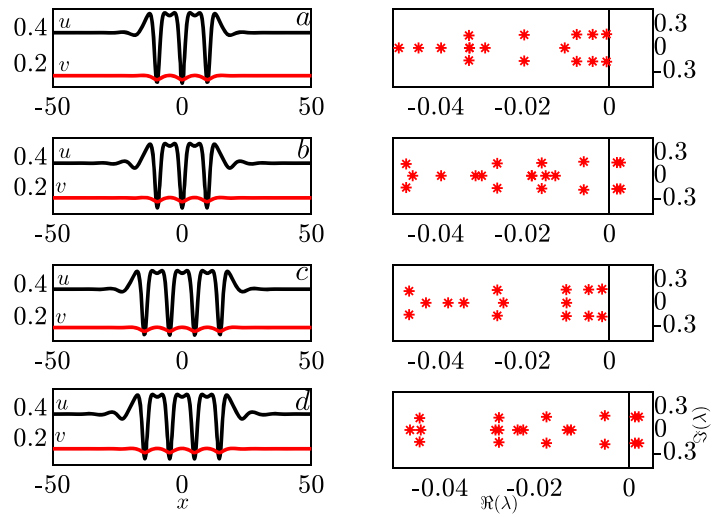

FIG. 5. Numerical spectral analysis of the localized patterns at the points labeled (a) to (d) in Fig. 4. (Left): solution profiles. (Right): the largest few temporal eigenvalues of the problem linearised about these profiles; all other eigenvalues have real parts that are more negative.

the instability is indeed inherited by the localized states but not at the same parameter values (cf. the location of the green dots in Fig. 4 and the vertical line $\alpha = \alpha_H$). At each of the green circles, we have

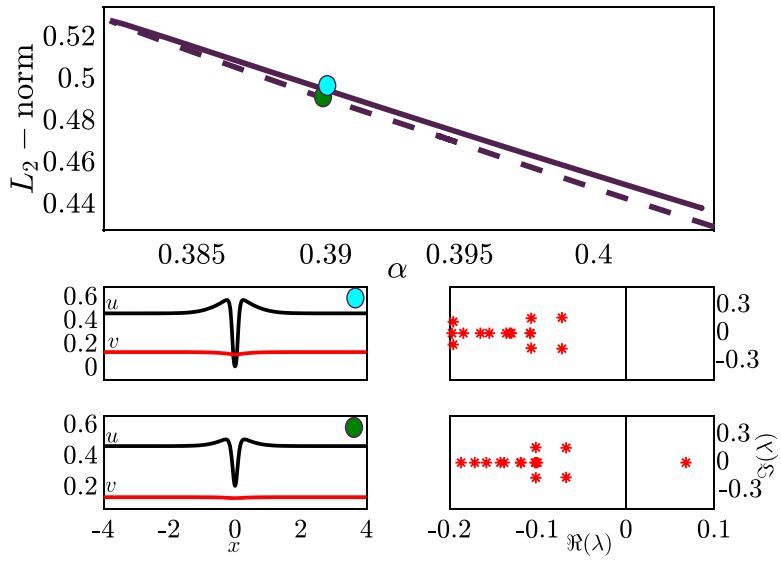

FIG. 6. (Top): numerical bifurcation diagram with α of the single-patch state for $\epsilon = 0.01$. The continuous/dashed line indicates stable/unstable solutions. (Lower plots): solution profiles at the coloured points with their corresponding eigenvalues with largest real parts.

found that the complex eigenvector that corresponds to the complex conjugate pair of eigenvalues that cross the imaginary axis is indeed a global, approximately spatially homogeneous, mode corresponding to the associated eigenvector of the Hopf bifurcation of the homogeneous state (result not shown).

Interestingly, the lowest part of the red curve in Fig. 4, which corresponds to the primary, single pulsed solution has its Hopf bifurcation at α_H. Where all other multi-patch solutions on the snaking curve have their Hopf instability at α-values that are less than α_H, which means that they destabilize while the background state is still stable. What happens beyond the Hopf instability forms the subject of the next subsection.

Before investigating more complex spatio-temporal behaviour, Fig. 6 completes the bifurcation picture for localized solutions, by showing the one-parameter diagram with α of a single-patch solution, below the BD curve. The depicted curve of solutions lies exclusively below the Hopf bifurcation line for the parameter values chosen. Here, there is a single fold that connects a larger-amplitude (stable) solution to a smaller amplitude (unstable) one. Such a solution structure could presumably be predicted in the limit $\epsilon \to 0$ using so-called semi-strong interaction theory in the spirit of Ward & Wei (2002), as recently shown for a Schnakenberg-like model in Al Saadi *et al.* (2021a). Note that the only instability detected here is the fold, but the analysis in Al Saadi *et al.* (2021a) suggests that for very small values of ϵ there may be another kind of Hopf bifurcation, which corresponds to a localized eigenvector. We shall not explore that singular limit further here.

3.4 *Onset of spatio-temporal chaos*

Using the snaking diagram in Fig. 4, we choose six values of α from the odd/even (red/blue) curve in the vicinity of the Hopf bifurcation to numerically generate Fig. 7. Here we carefully choose the parameter values and initial conditions so that α is on the stable side of the corresponding Hopf bifurcation which

are shown in plots (a) and (d), just beyond the Hopf bifurcation which are displayed in plots (b) and (e) and a little further beyond the bifurcation point that are depicted in plots (c) and (f). It should be noted that the α values used in (a)–(c) are from the odd curve while (d)–(f) are values taken from the even curve. In each case, we plot the results of the simulation as a heat map (upper part) and as the time series of the u-value at a single point in the domain.

From these simulations, we notice that the Hopf bifurcation for both kinds of solution is supercritical. That is, just beyond the bifurcation point there is a stable limit cycle. Moreover, as can be seen from the close inspection of the heat map plot, this limit cycle is a kind of 'breather' solution where all points in the domain are subject to amplitude modulation. We find that this limit cycle only exists for a narrow parameter window, as the amplitude of the oscillation changes rapidly with $\alpha - \alpha_H$. In each of the branches, we find that a secondary instability occurs in which outer patches collapse. This leads to what appears to be spatio-temporal chaos that is somehow reminiscent of weak turbulence in which the trajectory intermittently visits neighbourhoods of states with different numbers of localized patches. For much higher values of α, the solution is observed to become more irregular.

4. Two-dimensional simulation results

A natural question arises whether analogues of the kind of structures we have observed in one spatial dimension exists in 2D. To seek a preliminary answer, we have performed numerical simulations using second-order finite differences on a square domain $(x, y) \in [0, L] \times [0, L]$, using Neumann boundary conditions. As with the 1D simulations, we solve the resulting large system of ordinary differential equations (ODEs) in time using Matlab's `ode15s` again taking care to choose stepsizes that avoid numerical instability. The domain size L is chosen to be sufficiently large such that obvious boundary effects do not apply. Moreover, we retain the parameter values (3.1) from the 1D case while varying α and ϵ. Nevertheless, the computational results are intended to be illustrative rather than exhaustive.

First, we choose values of ϵ and α from below the Hopf bifurcation curve in Fig. 3, where the 1D model has attractors that are steady pattern states. Figure 8a shows corresponding 2D solutions from the isolated patch region, Fig. 8b shows a solution corresponding to a localized patterned state and Fig. 8c shows a spatially periodic solution from inside the Turing region. In these plots, we show the concentration of prey as a coloured map. It can be seen that as we move from the isolated patch region through to the snake region and then to the Turing region, there is an increase in the density of depleted-prey patches.

Figure 9 in contrast shows the results of similar simulations for parameter values which correspond in the 1D case to being above the Hopf-bifurcation line but in the localized pattern region. The upper plots, Fig. 9a–c shows three different time-slices of the prey field plot as a colour map from a particular initial condition which has a single depleted prey patch within a background close to S_3. We have used other initial conditions in this parameter region and have found no evidence that the simulation reaches any steady state, other than the trivial one S_3 for small enough perturbations from it. For sufficiently large perturbations, we find that these non-repeating dynamics appear to be spatio-temporally chaotic. This chaotic dynamics is further indicated by the time series of Fig. 9d, which shows the u-field at a single point in space.

5. Results for a related model

To reinforce that what we have observed is in some way generic to a class of predator–prey models, we shall briefly indicate results for a further model with a different nonlinearity, namely a Holling type-III

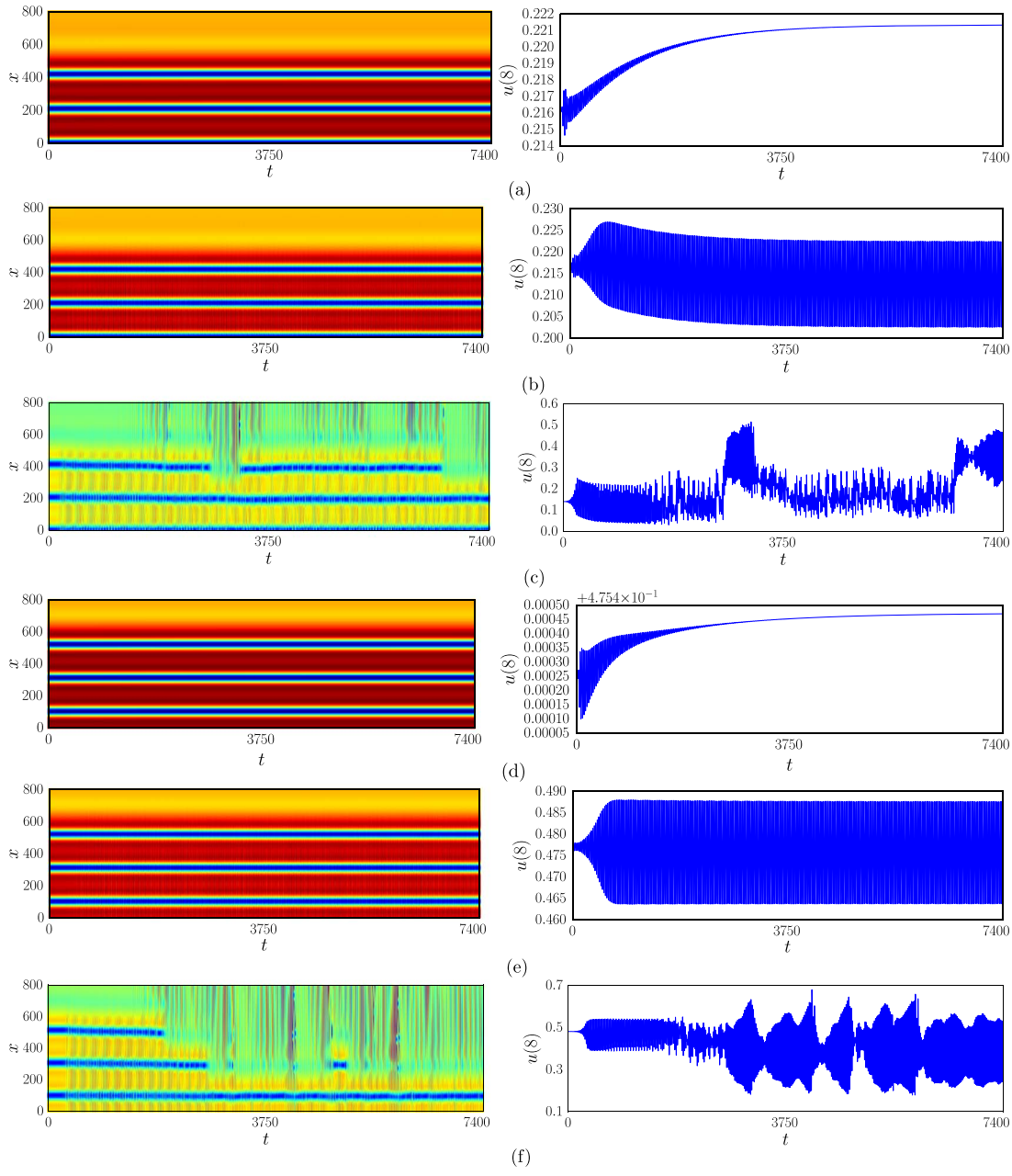

FIG. 7. Numerical simulation of (2.1) depicted as a heat map of the u component (red/blue are higher/lower amplitude values) on left and time series of the point $u(8)$ on right for six different values of α from branches from Fig. 4 with odd and even numbers of patches, by fixing $\epsilon = 0.085$ using the following: (a) $\alpha = 0.41025$, (b) $\alpha = 0.4105$, (c) $\alpha = 0.4135$, (d) $\alpha = 0.4103$, (e) $\alpha = 0.41055$ and (f) $\alpha = 0.4135$.

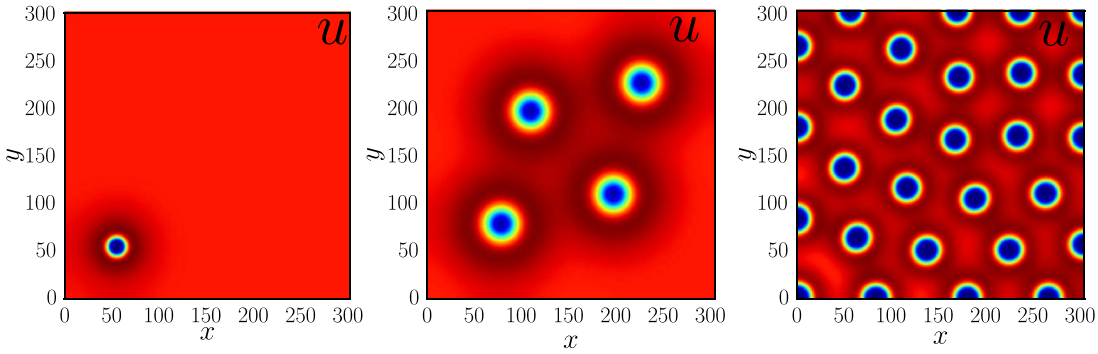

(a) (b) (c)

FIG. 8. Two-dimensional solution patterns obtained by numerical simulation of (2.1). Figures represent typical pattern solutions at the following parameter values: (a) a single spike for $(\epsilon, \alpha) = (0.01, 0.39)$, (b) a localized pattern at $(\epsilon, \alpha) = (0.05, 0.4)$ and (c) a periodic-Turing pattern with $(\epsilon, \alpha) = (0.02, 0.41)$.

predator–prey model. This model was studied in Wang (2010) who found evidence for Turing instability, travelling waves and stationary patches. Our aim is to show that a similar bifurcation diagram applies here too.

The model in question is represented by the following system of nonlinear PDEs:

$$u_t = u(1-u) - \frac{\alpha u^2 v}{v^2 + u^2} + \epsilon \nabla^2 u, \quad t > 0, \tag{5.1a}$$

$$v_t = \frac{\beta u^2 v}{v^2 + u^2} - \delta v + \nabla^2 v, \quad t > 0, \tag{5.1b}$$

subject to Neumann boundary conditions. For simplicity, we shall present results only in 1D, for $x \in (-L, L)$, with $L \gg 1$. The positive parameters have similar meaning as they did in 2.1; α denotes the consumption rate of the prey by the predators, β is the half-saturation constant, δ is the death rate of the predator and $\epsilon \ll 1$ is the prey to predator diffusion ratio.

The model has many similar properties to (2.1) and can be analysed similarly. We omit most of the details. There are again three spatially homogeneous equilibria: $S_1(0,0)$, $S_2(1,0)$ and $S_3(u^*, v^*)$ where

$$u^* = \frac{\beta - \xi}{\beta}, \quad v^* = \frac{u^* \xi}{\alpha \delta}, \quad \xi = \sqrt{\alpha^2 \delta (\beta - \delta)}.$$

Note that both components are positive if $\beta > \delta$ and $\beta > \xi$, which is a constraint on the parameters in order for the coexistence state to exist.

Figure 10a presents the linear and weakly nonlinear analysis, which is presented in exactly the same ways as Fig. 3. We note that the results are qualitatively highly similar to those of the previous model. Numerical simulation has also indicated the oscillatory behaviour above the Hopf bifurcation line.

Interestingly, even though the qualitative results are similar, the models cannot be mapped onto one another by any simple transformation, owing to the different powers in the interaction terms. Also, note

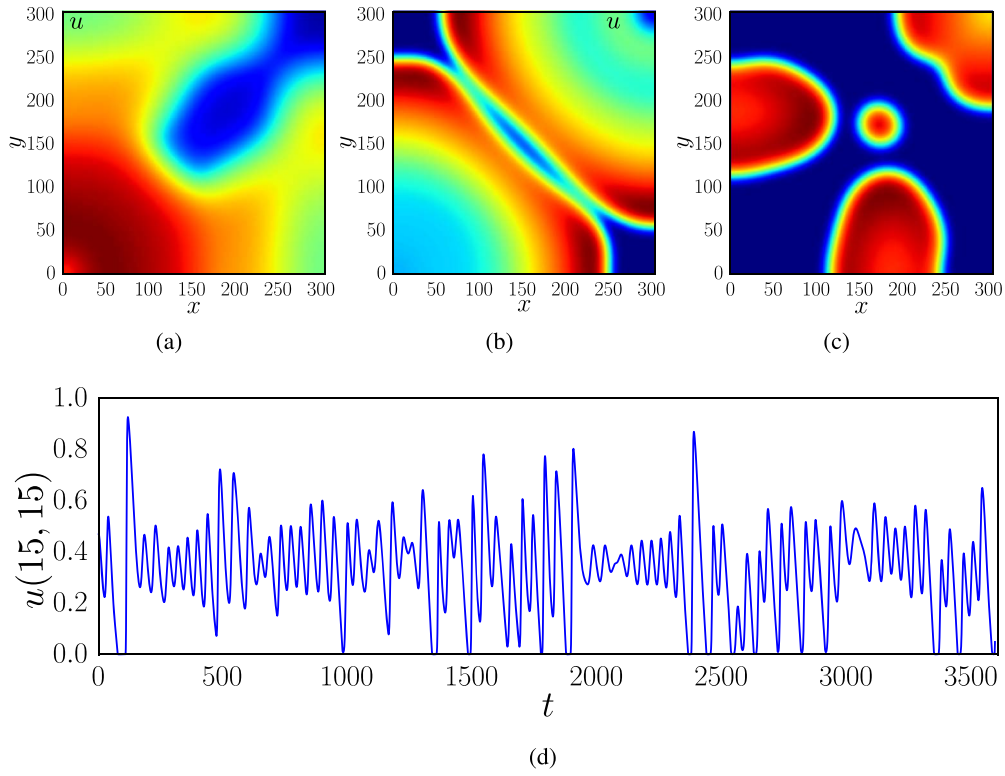

FIG. 9. Two-dimensional solution patterns by numerically solving (2.1). Figures represent typical pattern solutions in the snaking region with parameter values $(\epsilon, \alpha) = (0.125, 0.416)$ at three different time steps: (a) $t = 200$; (b) $t = 1700$; (c) $t = 3500$ and (d) time evolution of the u-field at a single point in the domain $(x, y) = (15, 15)$.

the differences in the values of the parameters in Figs 3 and 10a. Thus, the similarity between results points to a certain generality to the bifurcation structures revealed.

6. Discussion

The purpose of this paper has been to systematically investigate the propensity of predator–prey systems to develop spatially localized dynamics, without the need for any spatial heterogeneity. Although, previous studies have explored spatio-temporal dynamics of predator–prey models within the Turing–Hopf region (as outlined in the Introduction) we believe this is the first attempt at a systematic study showing how spatially localized structures can occur on large domains.

Specifically, a suite of tools that combines linear and nonlinear analysis with numerical continuation and simulation has been used to obtain qualitative two-parameter bifurcation diagrams for two different reaction–diffusion predator–prey models. Our aim has been to uncover the specific behaviour of models of particular ecological systems but that of a wide class of predator–prey models. Also, rather than exhaustive numerical studies, we have sought to explain a general morphology of the bifurcation diagram of such systems.

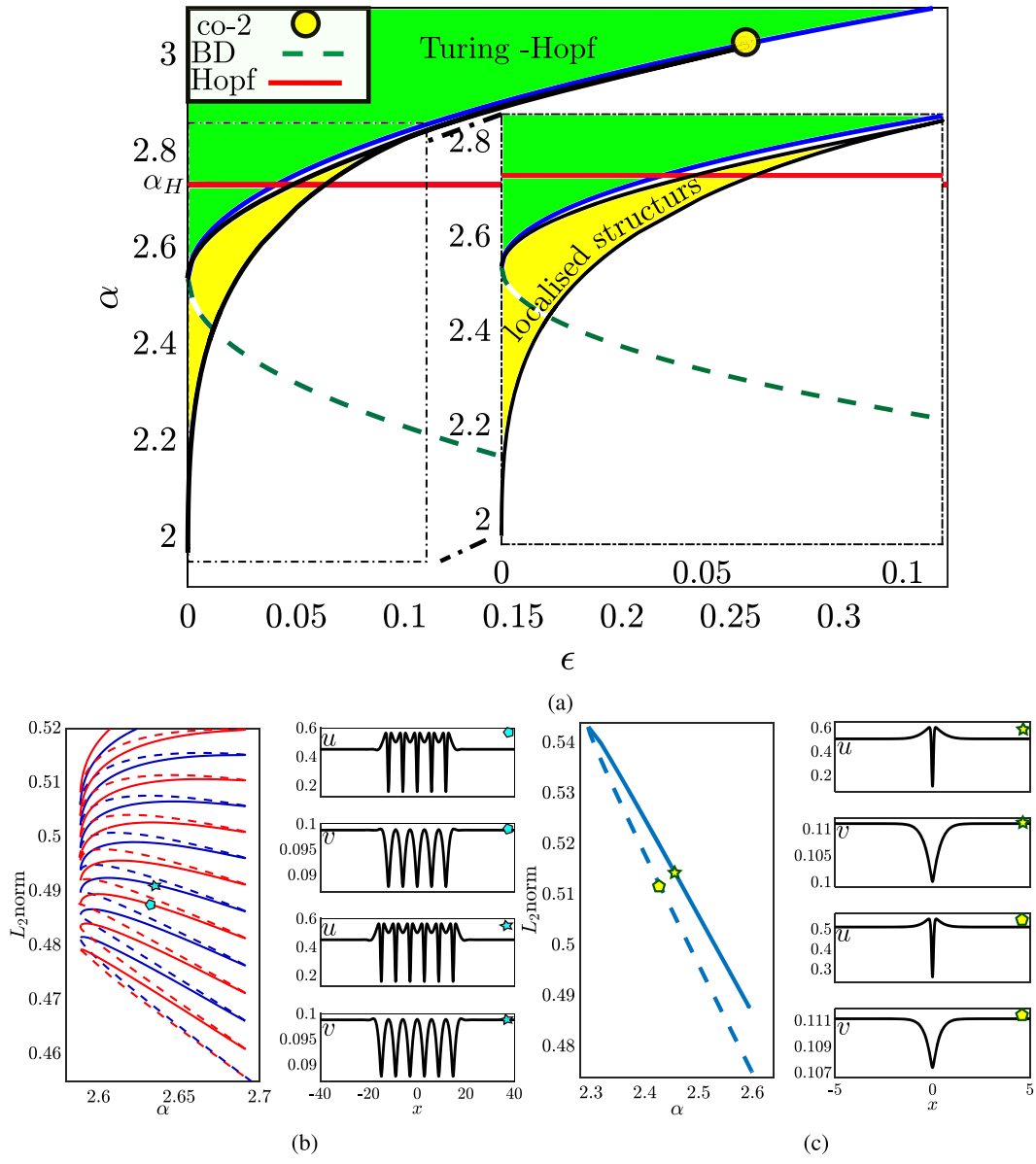

FIG. 10. (a) Two-parameter bifurcation diagram of steady solutions to (5.1) in the (ϵ, α)-plane for fixed $\delta = 0.86$ and $\beta = 0.9$. The meaning of colours and symbols is as in Fig. 3, as is the method of computation. (b) Homoclinic snaking for $\epsilon = 0.03$ as α varies. The continuous (dashed) line indicates stable (unstable) solution, whereas red (blue) indicates that the number of peaks in the solution is odd (even). Two stable solutions with different number of peaks marked by the hexagon and star in the snaking diagram are shown alongside. (c) One-parameter continuation of the single patch solution for $\epsilon = 0.004$, showing a stable large-amplitude state being connected to an unstable lower-amplitude one via a fold.

In particular, we have shown that as we approach the singular limit that the ratio of diffusion constants between prey and predator tends to zero, then the fundamental Turing bifurcation of the coexistence equilibrium becomes subcritical. This leads to a pinning region between background and patterned states within which localized structures are known to occur via the homoclinic snaking mechanism. Remarkably, the global bifurcation structure of stationary patterns in two parameters is found to follow a similar pattern to that recently observed (Al Saadi *et al.*, 2021a; Verschueren & Champneys, 2017, 2021) in Schnakenberg-type reaction-diffusion equations, which do not have a predator–prey structure. This suggests a certain ubiquity to these overall bifurcation structure, which will be further reported on elsewhere (Al Saadi *et al.*, 2021b).

A novel feature of predator–prey systems compared with Schnakenberg-type models is that the spatially homogeneous model can naturally undergo Hopf bifurcation in addition to a Turing instability. Thus, we have deliberately chosen parameter values in which this Hopf bifurcation interacts with the region in which the subcritical Turing bifurcation and localized structures exist. This led to interesting novel observations on the nature of the Hopf bifurcations occurring on branches of localized steady states. These were found to all be supercritical, yet to occur for parameter values that are different from that of the homogeneous Hopf bifurcation. We also found that the Hopf bifurcation gives a route to localized spatio-temporal chaos within this parameter region. It would be interesting in future work to consider an unfolding of the codimension-three point where the super- to subcritical Turing bifurcation transition occurs simultaneously with the Hopf bifurcation.

Most of our results were presented in one spatial dimension. Although much remains to be done to explore these mechanisms in 2D, we nevertheless provided evidence of two-dimensional analogues of these 1D structures occurring at similar parameter values.

This paper is not primarily designed to contribute to practical understanding of spatial ecology. Nevertheless, there is one broad conclusion, namely that the observation of spatially localized patterns of high or low species concentrations (whether spatial or spatio-temporal) do not necessarily imply the existence of spatial heterogeneous causes. Specifically, within the simplest generic predator–prey models there are parameter regimes where the Turing bifurcation is subcritical and localized patterns are to be expected. In the models we have studied, the parameter limit in question requires that the prey is relatively static while the predator diffuses more rapidly. One particular application of this limit could be the existence of localized vegetation patches in an arid environment where the prey is associated with the vegetation ecosystem which the predator is associated with the wider environment of the region; see e.g. Borgogno *et al.* (2009), Bordeu *et al.* (2016) and Cobbold *et al.* (2015).

Acknowledgements

We should also like to thank an anonymous referee for bringing further useful references on spatial ecology to our attention.

Funding

Ministry of Higher Education, Research and Innovation Oman (to F.A.S.); Military Technological College Oman (to F.A.S.).

References

Al Saadi, F., Champneys, A., Gai, C. & Kolokolnikov, T. (2021a) Spikes and localised patterns for a novel Schnakenberg model in the semi-strong interaction regime. *Eur. J. Appl. Math.*, 1–20. doi: 10.1017/S0956792520000431.

Al Saadi, F., Champneys, A. & Verschueren, N. (2021b) Localised patterns and semi-strong interaction, a unifying framework for reaction-diffusion systems (in press).

Bandyopadhyay, M. & Chattopadhyay, J. (2005) Ratio-dependent predator–prey model: effect of environmental fluctuation and stability. *Nonlinearity*, **18**, 913–936.

Banerjee, M. & Petrovskii, S. (2011) Self-organised spatial patterns and chaos in a ratio-dependent predator–prey system. *Theor. Ecol.*, **4**, 37–53.

Banerjee, M. & Volpert, V. (2017) Spatio-temporal pattern formation in Rosenzweig–Macarthur model: effect of nonlocal interactions. *Ecol. Complexity*, **30**, 2–10.

Bastiaansen, R., Carter, P. & Doelman, A. (2019) Stable planar vegetation stripe patterns on sloped terrain in dryland ecosystems. *Nonlinearity*, **32**, 2759–2814.

Bastiaansen, R., Jaibi, O., Deblauwe, V., Eppinga, M., Siteur, K., Siero, E., Mermoz, P., Bouvet, A., Doelman, A. & Rietkerk, M. (2018) Multistability of model and real dryland ecosystems through spatial self-organization. *Proc. Natl. Acad. Sci. U. S. A.*, **115**, 11256–11261.

Beck, M., Knobloch, J., Lloyd, D., Sandstede, B. & Wagenknecht, T. (2009) Snakes, ladders, and isolas of localized patterns. *SIAM J. Math. Anal.*, **41**, 936–972.

Berezovskaya, F., Karev, G. & Arditi, R. (2001) Parametric analysis of the ratio-dependent predator–prey model. *J. Math. Biol.*, **43**, 221–246.

Bordeu, I., Clerc, M., Couteron, P., Lefever, R. & Tlidi, M. (2016) Self-replication of localized vegetation patches in scarce environments. *Sci. Rep.*, **6**, 33703.

Borgogno, F., D'Odorico, P., Laio, F. & Ridolfi, L. (2009) Mathematical models of vegetation pattern formation in ecohydrology. *Rev. Geophys.*, **47**, RG1005.

Champneys, A. (1998) Homoclinic orbits in reversible systems and their applications in mechanics, fluids and optics. *Phys. D*, **112**, 158–186.

Champneys, A., Al Saadi, F., Breña Medina, V., Grieneisen, V., Marée, A., Verschueren, N. & Wuyts, B. (2021) Bistability, wave pinning and localisation in natural reaction–diffusion systems. *Phys. D*, **416**, 132735.

Cobbold, C. A., Lutscher, F. & Sherratt, J. A. (2015) Diffusion-driven instabilities and emerging spatial patterns in patchy landscapes. *Ecol. Complexity*, **24**, 69–81.

Cross, M. & Hohenberg, P. (1993) Pattern formation outside of equilibrium. *Rev. Modern Phys.*, **65**, 851–1112.

Dawes, J. & Souza, M. (2013) A derivation of holling's type I, II and III functional responses in predator–prey systems. *J. Theor. Bio.*, **327**, 11–22.

Dawes, J. & Williams, J. (2016) Localised pattern formation in a model for dryland vegetation. *J. Math. Biol.*, **73**, 63–90.

Elphick, C., Tirapegui, E., Brachet, M., Coullet, P. & Iooss, G. (1987) A simple global characterization for normal forms of singular vector fields. *Phys. D*, **29**, 95–127.

Fletcher, R. & Fortin, M. (2018) *Spatial Ecology and Conservation Modelling. Applications with R*. Berlin: Springer.

Gandhi, P., Werner, L., Iams, S., Gowda, K. & Silber, M. (2018) A topographic mechanism for arcing of dryland vegetation bands. *J. Roy. Soc. Interface*, **15**, 20180508.

Grindrod, P. (1988) Models of individual aggregation or clustering in single and multi-species communities. *J. Math. Biol.*, **26**, 651–660.

Grindrod, P. (1996) *The Theory and Applications of Reaction–Diffusion Equations: Patterns and Waves*, 2nd edn. Oxford: OUP.

Haragus, M. & Iooss, G. (2007) *Local Bifurcations, Center Manifolds and Normal Forms in Infinite Dimensional Dynamical Systems*. New York: Springer.

Holling, C. (1959) Some characteristics of simple types of predation and parasitism. *Can. Entomol.*, **91**, 385–398.

Holling, C. S. (1965) The functional response of predators to prey density and its role in mimicry and population regulation. *Mem. Ent. Soc. Can.*, **97**, 5–60.

Hsu, S.-B., Hwang, T. W. & Kuang, Y. (2001) Global analysis of the Michaelis–Menten-type ratio-dependent predator–prey system. *J. Math. Biol.*, **42**, 489–506.

Jiang, X., She, Z., Feng, Z. & Zheng, X. (2017) Bifurcation analysis of a predator–prey system with ratio-dependent functional response. *Int. J. Bifurcation Chaos*, **27**, 1750222.

Knobloch, E. (2015) Spatial localization in dissipative systems. *Annu. Rev. Condens. Matter Phys.*, **6**, 325–359.

Kozyreff, G. & Chapman, S. (2006) Asymptotics of large bound state of localised structures. *Phys. Rev. Lett.*, **97**, 044502.

Kuang, Y. & Beretta, E. (1998) Global qualitative analysis of a ratio-dependent predator–prey system. *J. Math. Biol.*, **36**, 389–406.

Lejeune, O., Tlidi, M. & Couteron, P. (2002) Localized vegetation patches: a self-organized response to resource scarcity. *Phys. Rev. E*, **66**, 010901.

Lloyd, D. J. & O'Farrell, H. (2013) On localised hotspots of an urban crime model. *Phys. D*, **253**, 23–39.

Maini, P., Painter, K. & Nguyen Phong Chau, H. (1997) Spatial pattern formation in chemical and biological systems. *J. Chem. Soc. Faraday Trans.*, **93**, 3601–3610.

Medvinsky, A. B., Petrovskii, S. V., Tikhonova, I. A., Malchow, H. & Li, B.-L. (2002) Spatiotemporal complexity of plankton and fish dynamics. *SIAM Rev.*, **44**, 311–370.

Meron, E. (2015) *Nonlinear Physics of Ecosystems*, 3rd edn. CRC Press.

Meron, E. (2016) Pattern formation—a missing link in the study of ecosystem response to environmental changes. *Math. Biosci.*, **271**, 1–18.

Meron, E. (2018) From patterns to function in living systems: dryland ecosystems as a case study. *Annu. Rev. Condens. Matter Phys.*, **9**, 79–103.

Meron, E. (2019) Vegetation pattern formation: the mechanisms behind the forms. *Phys. Today*, **72**.

Mukherjee, N., Ghorai, S. & Banerjee, M. (2018) Effects of density dependent cross-diffusion on the chaotic patterns in a ratio-dependent prey-predator model. *Ecol. Complexity*, **36**, 276–289.

Murray, J. (2002) *Mathematical Biology II: Spatial Models and Biomedical Applications*, 3rd edn. New York: Springer.

Okubu, A. & Levin, S. (2001) *Diffusion and Ecological Problems: Modern Perspectives*. New York: Springer.

Pascual, M. (1993) Diffusion-induced chaos in a spatial predator & prey system. *Philos. Trans. R. Soc. Lond. B Biol. Sci.*, **251**, 1–7.

Potts, J. & Lewis, M. (2019) Spatial memory and taxis-driven pattern formation in model ecosystems. *Bull. Math. Biol.*, **81**, 1–23.

Rosenzweig, M. (1971) Paradox of enrichment: destabilization of exploitation ecosystems in ecological time. *Science*, **171**, 385–387.

Rosenzweig, M. & MacArthur, R. (1963) Graphical representation and stability conditions of predator–prey interactions. *Am. Nat.*, **97**, 209–223.

Roy, S. & Chattopadhyay, J. (2007) The stability of ecosystems: a brief overview of the paradox of enrichment. *J. Biosci.*, **32**, 421–428.

Ruiz-Reynés, D., Gomila, D., Sintes, T., Hernández-García, E., Marbà, N. & Duarte, C. M. (2017) Fairy circle landscapes under the sea. *Sci. Adv.*, **3**, e1603262.

Sandstede, B. (1997) Convergence estimates for the numerical approximation of homoclinic solutions. *IMA J. Numer. Anal.*, **17**, 437–462.

Skellam, J. G. (1951) Random dispersal in theoretical populations. *Biometrika*, **38**, 196–218.

Taylor, N., Kim, H., Krause, A. & Van Gorder, R. (2020) A non-local cross-diffusion model of population dynamics i: emergent spatial and spatiotemporal patterns. *Bull. Math. Biol.*, **82**, 112.

Tes, W. H. & Ward, M. J. (2016) Hotspot formation and dynamics for a continuum model of urban crime. *European J. Appl. Math.*, **27**, 583–624.

Tilman, D. & Kareiva, P. (1997) *Spatial ecology: the role of space in population dynamics and interspecific interactions*. Princeton, NJ: Princeton University Press.

Verschueren, N. & Champneys, A. (2017) A model for cell polarization without mass conservation. *SIAM J. Appl. Dyn. Syst.*, **16**, 1797–1830.

Verschueren, N. & Champneys, A. (2021) Dissecting the snake: transition from localized patterns to spike solutions. *Phys. D*, **419**, 132858.

Wang, L. (2010) Spatial pattern formation of a ratio-dependent predator prey model. *Chin. Phys. B*, **19**, 090206.
Ward, M. & Wei, J. (2002) The existence and stability of asymmetric spike patterns for the Schnakenberg model. *Stud. Appl. Math.*, **109**, 229–264.
Woods, P. & Champneys, A. (1999) Heteroclinic tangles and homoclinic snaking in the unfolding of a degenerate reversible Hamiltonian–Hopf bifurcation. *Phys. D*, **129**, 170–174.
Wuyts, B., Champneys, A. & House, J. (2017) Amazonian forest-savanna bistability and human impact. *Nat. Commun.*, **8**, 15519.
Xiao, D. & Jennings, L. S. (2005) Bifurcations of a ratio-dependent predator–prey system with constant rate harvesting. *SIAM J. Appl. Math.*, **65**, 737–753.
Xiao, D. & Ruan, S. (2001) Global dynamics of a ratio-dependent predator–prey system. *J. Math. Biol.*, **43**, 268–290.
Zelnik, Y. R., Kinast, S., Yizhaq, H., Bel, G. & Meron, E. (2013) Regime shifts in models of dryland vegetation. *Philos. Trans. R. Soc. Lond. Ser. A*, **371**, 20120358.
Zelnik, Y. R., Meron, E. & Bel, G. (2016) Localized states qualitatively change the response of ecosystems to varying conditions and local disturbances. *Ecol. Complexity*, **25**, 26–34.